

HiL Demonstration of Online Battery Capacity and Impedance Estimation with Minimal a Priori Parametrization Effort

Camiel J.J. Beckers*, Feye S.J. Hoekstra*, Frank Willems*†

*Powertrains Dept., TNO Mobility & Built Environment, Helmond, The Netherlands, Email: camiel.beckers@tno.nl

† Department of Mechanical Engineering, Eindhoven University of Technology, Eindhoven, The Netherlands

Abstract—Uncertainty in the aging of batteries in battery electric vehicles impacts both the daily driving range as well as the expected economic lifetime. This paper presents a method to determine online the capacity and internal resistance of a battery cell based on real-world data. The method, based on a Joint Extended Kalman Filter combined with Recursive Least Squares, is computationally efficient and does not a priori require a fully characterized cell model. Offline simulation of the algorithm on data from differently aged cells shows convergence of the algorithm and indicates that capacity and resistance follow the expected trends. Furthermore, the algorithm is tested online on a Hardware-in-the-Loop setup to demonstrate real-time parameter updates in a realistic driving scenario.

Index Terms—State-of-Health (SoH), Parameter Estimation, Battery Management System (BMS), Hardware-in-the-Loop (HiL), Forgetting-Factor Recursive Least-Squares (FFRLS)

I. INTRODUCTION

In an effort to reduce greenhouse gas emissions, the world is transitioning to electric mobility. Many of these new energy vehicles rely on lithium-ion batteries as their primary energy carrier. To ensure safe and reliable operation, a Battery Management System (BMS) monitors the battery cells and enforces strict operational boundaries. One of the challenging aspects of battery management is that the battery capacity and impedance can change and degrade over time and use, which shortens the driving range of the vehicle and can potentially impact safety. Moreover, upcoming EU regulations concerning battery traceability, i.e., the battery passport, require manufacturers to provide up-to-date battery health information. Therefore, accurate tracking of the capacity and impedance is crucial.

Given its importance, the separate topics of impedance and capacity estimation, but in particular also joint, i.e., integrated, solutions have received significant attention in literature. A high variety of solutions exists; Some apply electrochemical impedance-spectroscopy, see, e.g., [1], where capacity is linked to particular impedance responses, thus providing a fast capacity estimate. Others apply scanning for particular changes in operational characteristics such as repeated

charge curves [2]. In recent years, many machine learning approaches have also surfaced ranging from straight-forward support vector machines to artificial neural networks [3]. Nevertheless, the most described approach for impedance and capacity estimation is some form of a joint state and parameter estimator in combination with a Least Squares (LS) estimator for the capacity based on the difference in estimated State-of-Charge (SoC) and integrated current.

While seemingly straightforward, there exist many combinations or stand-alone implementations of these two options. In this paragraph, a brief impression is provided of the various options. For instance, in [4], capacity is estimated using a total LS structure, which shows accurate capacity estimation, but presents an unfair comparison with ordinary LS and requires a significant number of evaluations. Similarly, capacity is estimated in a recursive fashion based on small SoC segments in [5], but updating of impedance parameters is not considered. On the other hand, in [6], an adaptive Extended Kalman Filter (EKF) is applied to estimate the states, i.e., SoC and overpotential, in combination with two separate LS estimators for estimating model parameters and capacity. Lastly, in [7], LS is not applied, but instead, capacity is integrated into the EKF by adding aging dynamics to the model structure. While potentially powerful, it requires significant a priori parametrization effort. Overall, these implementations focus on estimating either capacity or impedance but not both or require significant modeling effort prior to deployment.

In this paper, a Joint Extended Kalman Filter (JEKF) with forgetting factor, estimating SoC, overpotential, and only two model parameters, is paired with an ordinary LS capacity estimator with forgetting factor which is evaluated only once per (dis)charging segment, automatically triggered by cycle detection logic. This coupled structure, constituted of pre-existing structures for separate estimation of impedance and capacity altered with seemingly minor yet important changes, provides computationally inexpensive impedance and capacity estimation while requiring minimal parameterization prior to deployment. The coupled estimation structure is tested on dynamic excitation data measured at several stages of aging for the same cell, and the results demonstrate a consistent relation with impedance increase, capacity decrease, and cell age. Lastly, this structure has been deployed in a Hardware-

This work has received financial support from the Dutch Ministry of Economic Affairs and Climate, under the grant ‘R&D Mobility Sectors’ and as part TNO’s Early Research Program in the scope of the project ‘AUTO ADAPT’.

in-the-Loop (HiL) setting and the results verify the offline performance.

II. SIMULTANEOUS STATE, PARAMETER, AND CAPACITY ESTIMATION

Before diving deeper into the capacity and parameter estimation approach, let us first discuss the model structure at hand. In this paper, we consider the battery to be modeled by a first-order dynamical system given by

$$\begin{bmatrix} s_{k+1} \\ o_{k+1} \end{bmatrix} = \begin{bmatrix} 1 & 0 \\ 0 & \theta_1 f_1(\mathbf{p}_k) \end{bmatrix} \begin{bmatrix} s_k \\ o_k \end{bmatrix} + \begin{bmatrix} \frac{\tau}{C_0} \\ \theta_2 f_2(\mathbf{p}_k) \end{bmatrix} u_k, \quad (1a)$$

$$\hat{y}_k = g(s_k) + o_k + \theta_3 f_3(\mathbf{p}_k) u_k, \quad (1b)$$

with $k \in \mathbb{Z}^+$ the time, s_k the SoC, o_k the dynamic part of the overpotential, u_k the applied current and \hat{y}_k the predicted terminal voltage. Furthermore, $g(s_k)$ is a monotonic function representing the Electromotive-Force (EMF), also known as open-circuit voltage, C_0 [As] is the battery capacity, $\theta_1 f_1(\mathbf{p}_k)$ is the overpotential relaxation rate, $\theta_2 f_2(\mathbf{p}_k)$ the overpotential increase due to the applied current and $\theta_3 f_3(\mathbf{p}_k)$ models the Ohmic resistance and all high-frequency impedances, i.e., faster than the sampling time τ . Here, f_i with $i \in \{1, 2, 3\}$ are functions of $\mathbf{p}_k = \{p_0, \dots, p_k\}$ representing one or multiple scheduling variables. Essentially, $\theta_i f_i(\mathbf{p}_k)$ is a pre-parametrised function multiplied with a scaling factor θ_i . In this way, the dependency of system dynamics on, e.g., SoC or temperature, can be incorporated while maintaining adaptability with respect to aging or model uncertainty. In the remainder of this paper, we assume free system dynamics, i.e., $f_i(\mathbf{p}_k) = 1$ for all i .

Note that system (1) is fully equivalent to a 1-RC pair equivalent-circuit model, with series resistance R_0 , and RC pair resistance R_1 and capacitance C_1 , with exact equivalence given by

$$R_0 = \theta_3, \quad (2)$$

$$R_1 = -\theta_2 / (\theta_1 - 1), \quad (3)$$

$$C_1 = -(e^{-t_s} (\theta_1 - 1)) / (\theta_1 \theta_2). \quad (4)$$

Considering system (1), we can now formalize the goal of capacity and impedance tracking as

$$\min_{C_0, \theta_1, \theta_2, \theta_3} \sum_{k \in \mathcal{K}} (y_k - \hat{y}_k)^2, \quad (5)$$

with y_k the measured battery terminal voltage and samples $\mathcal{K} = \{1, \dots, K\}$ where K marks battery End-of-Life.

Solving (5) is non-trivial, let alone doing so in an online recursive fashion, which would be required on the BMS. This paper proposes an estimation structure consisting of two main elements, namely a JEKF with forgetting factor, as presented in [8], which estimates the SoC and the dynamical model parameters and the Recursive Least Squares (RLS) capacity estimator.

A. JEKF State and Parameter Estimation

The JEKF employed here is taken from [8], where the JEKF is combined with a forgetting factor which enables single-knob tuning, i.e., choosing the forgetting factor γ . The ‘joint’ aspect

of the Kalman filter implies that in addition to the internal model states, such as SoC, also model parameters are being estimated. In this case, only θ_2 and θ_3 will be estimated by the filter, unlike in [8], where all overpotential parameters are estimated. Incorrect estimation of θ_1 can occur in situations with poor observability [8], such as constant-current charging. Due to the severe consequences of incorrect estimation of θ_1 on model stability, namely if $\theta_1 > 1$ then (1) is unstable, θ_1 is chosen to be fixed. In this paper, a value of $\theta_1 = 0.99$ is chosen for a model sampling time of $\tau = 1$ s.

To estimate θ_2 and θ_3 online, system (1a) is extended according to

$$x_{k+1} = \begin{bmatrix} 1 & 0 & 0 \\ 0 & \theta_1 & 0 \\ 0 & 0 & I \end{bmatrix} x_k + \begin{bmatrix} \frac{\tau}{C_0} \\ \theta_{2,k} \\ 0 \end{bmatrix} u_k, \quad (6a)$$

$$\hat{y}_k = g(s_k) + o_k + \theta_{3,k} u_k, \quad (6b)$$

with $x_k = [s_k, o_k, \theta_{2,k}, \theta_{3,k}]^\top$ and $I = \text{diag}([1, 1])$ the identity matrix. In (6), the state vector has been extended with the, now time-varying, model parameters $\theta_{k+1} = \theta_k$. The dynamics for θ_1 are omitted for reasons mentioned above. The benefit of using (6), is that only limited prior knowledge, in the form of the EMF $g(s_k)$ and an estimate for θ_1 are required as input, while allowing for impedance increase, in the form of $\theta_{2,k}$ and $\theta_{3,k}$, as the battery ages. For details on the JEKF and how to select the forgetting factor γ , the reader is referred to [8].

B. Recursive Least Squares Capacity Estimation

Besides accommodating for impedance increase, it is crucial to track capacity fade by updating C_0 . In essence, similar to many others such as [5], [9], the capacity is estimated by comparing the difference in estimated SoC and the recorded difference in capacity throughput over a certain window, yielding a capacity estimate according to

$$\hat{C}_0 = \frac{\tau \sum_{k=a}^b u_k}{\hat{s}_b - \hat{s}_a}, \quad (7)$$

with a and b denoting the start and end time-instant of the window, respectively. In this paper, we consider a simple fading-memory ordinary least-squares optimization problem given by

$$\min_{\hat{C}_0} \sum_{j=1}^n \lambda^{n-j} \left(\tau \sum_{k=a_j}^{b_j} u_k - \hat{C}_0 (\hat{s}_{b_j} - \hat{s}_{a_j}) \right)^2, \quad (8)$$

where $\lambda \in [0, 1]$ is the forgetting factor, $n \in \mathbb{Z}^+$ the number of windows, and a_j and b_j the start and end time-instant of each window j . The optimal solution and its corresponding recursive form can be found in, e.g., [10]. Due to its simplicity, the ordinary least squares implementation is preferred here over alternatives such as total least squares. The merits of the latter, attributed to more complicated implementations, are often based on assumptions like Gaussian distributed errors in current sensing or SoC estimation. However, in practice these errors are often encountered to be of a more complicated nature such as biased current sensors, such as treated in [11], or skewed SoC estimates due to limitations of the

underlying model structure (1) or errors in the applied EMF realization $g(s_k)$. Therefore, and because it is most practical for implementation on embedded hardware, the authors opt for RLS with forgetting factor.

In this paper the window size is maximized by choosing a and b respectively as the start and end of charging sessions, thus reducing the number of evaluations of (7) to one per charging segment. Only continuous charging segments where $(\hat{s}_b - \hat{s}_a) > 0.2$ are considered. Not only does this result in a computational reduction, but it potentially minimizes the impact of SoC estimation errors on the estimate \hat{C}_0 , as will be shown in Section III. Namely, assuming the integration error of the current sensor is relatively small, the larger the difference between \hat{s}_a and \hat{s}_b , the smaller the impact of estimation errors will be. Note that more frequent evaluation is not likely to reduce impact of SoC estimation errors due to its non-zero mean nature.

III. RESULTS - SINGLE CELL WITH AGING

To demonstrate the performance of the JEKF and the effect of the iterative capacity updates, the proposed algorithm is evaluated over cycling data from an LG M50 21700 cell. For this cell, no other prior information is available except the EMF-curve $g(s_k)$, obtained from a C/20 discharge and its corresponding capacity C_0 . The data represents 10 WLTP-discharge-CC-charge cycles, which combined last 36 hours. This data is available at a sampling rate of 10Hz, yet is downsampled to 1 Hz before analysis. Lastly, the same cycling data is available at three stages of the cell's life while it was subject to aging tests: at Beginning of Life (Dec '21), at mid-life (Mar '22) and towards end-of-life (Jun '22). Between these moments, the cell was continuously cycled performing the described drivecycles at an ambient temperature of 25 °C.

A. JEKF Performance

To test the performance of the JEKF, as described in Section II-A, it is evaluated over the aforementioned beginning-of-life data. The JEKF is initialized with the initial state estimate $\hat{x}_0 = [s_0, 0, 10^{-4}, 0.02]^T$, where s_0 is determined by mapping the first voltage measurement to the SoC via the EMF $g(s_k)$. As implied by the initial overpotential $o_0 = 0$, the experiment is assumed to start in rest. Secondly, the covariance matrix of the JEKF is initialized as $P_0 = \text{diag}([1, 1, 10^{-6}, 4 \cdot 10^{-4}])$, which indicates the relatively large uncertainty which is placed on this relaxed-start assumption. The single-knob tuning factor is chosen as $\gamma = 0.999$ to allow for relatively fast changes in the parameters θ_2 and θ_3 .

Evaluating the JEKF over the beginning-of-life data without updating the capacity results in the blue lines in Fig. 1 and Fig. 2. Here, the results show that the JEKF converges to a plausible SoC value within the first minutes and that the JEKF tracks the terminal voltage of the cell well. The RMS value of the terminal voltage error, visualized in the bottom graph of Fig. 1, is 7.1 mV over the entire dataset.

1) *Capacity Estimation:* Next, the RLS algorithm is used to estimate capacity based on the charging segments, as described in Section II-B. For this, $\lambda = 0.7$ is chosen to enable fast

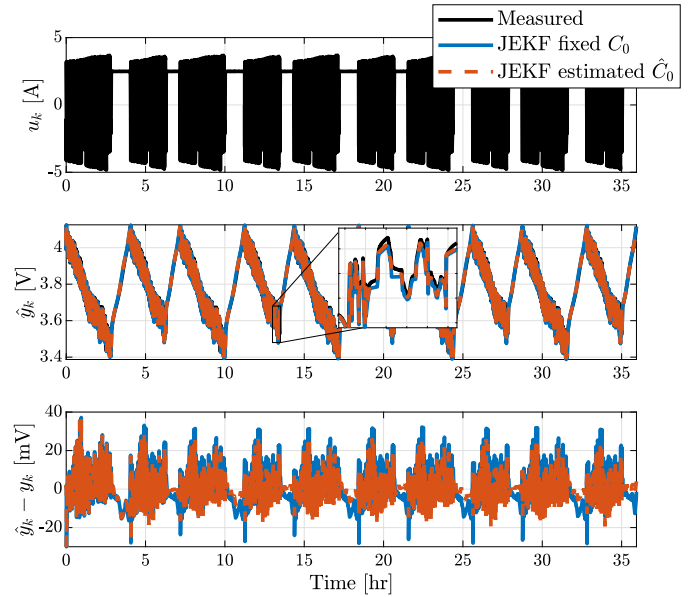


Fig. 1: The input current u_k and the estimated terminal voltage \hat{y}_k of the JEKF on 36 hours of WLTP data (beginning-of-life), both without and with capacity updates.

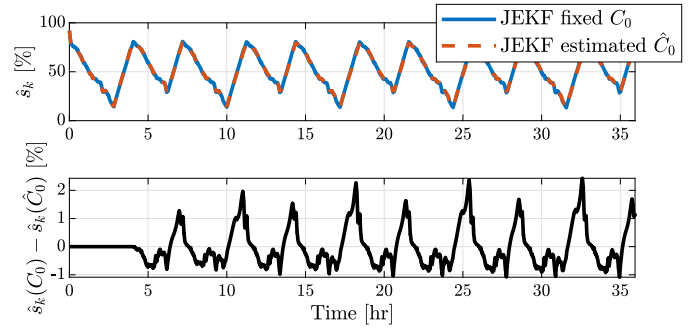


Fig. 2: The estimated SOC \hat{s}_k of the JEKF on 36 hours of WLTP data (beginning-of-life), both without and with capacity updates.

convergence of the RLS algorithm. The resulting capacity estimates are shown in Fig. 3, subfigure 1, which shows that the estimated capacity starts at the reference value of 4.4 Ah, and changes after the first CC charge is complete at around $t = 4$ hr. After this, small changes are applied every time a new CC charge is complete resulting in a final capacity estimate of 4.7 Ah. The resulting JEKF performance under the influence of these incremental capacity updates is displayed in Fig. 1 and Fig. 2 by the red, dashed line. The results show that initially, the output of both methods is the same, until after the first CC-charge, when the first capacity update occurs. After this moment, a difference in estimated SoC, shown in Fig. 2, starts to appear and the performance of the JEKF with estimated capacity improves, reducing the RMS voltage error to 5.2 mV.

2) *Impedance Estimation:* Fig. 3 shows the parameter estimates of the JEKF both with and without the incremental capacity updates. In the fixed-capacity case, indicated by the

blue line, the impedances θ_2 and θ_3 show evident variation. Most notable are the peaks in θ_3 during the CC charging sections. Without capacity updates, the average value of θ_3 is 18 m Ω . The parameter estimates for the algorithm with capacity updates are visualized in Fig. 3, red line, and indicate that θ_2 and θ_3 show less variation, with the notable peaks in θ_3 disappearing after the first charging segment, when the capacity is first updated. The mean value for θ_3 is 17.6 m Ω .

Additionally, Fig. 3 shows in yellow the results where θ_1 is estimated as part of the joint state vector, just as originally presented in [8], while also using the RLS algorithm to estimate \hat{C}_0 . The respective initial covariance value used is 10^{-7} . The results show that $\theta_1 > 1$ for a moment at $t = 4$ hr, after completion of the first CC charge. This goes paired with a negative value of θ_2 , both of which indicate marginal stability of the JEFK. After this, the values seem to stabilize. However, the deviations of θ_2 and θ_3 at $t = [32, 33.5]$ indicate that impedance parameters are challenging to estimate uniquely, especially during charging. These incorrect parameter values will affect the SoC estimated by the JEFK, and subsequently the capacity values estimated from it. This motivates the initial choice to keep a fixed value for $\theta_1 = 0.99$, which is kept for the remainder of this paper.

Note that the impedance-estimation performance can be further improved by pre-parameterizing functions $f_i(\mathbf{p}_k)$ in (1) to capture the dependency of impedance on the SoC, or additionally but less relevant for this data, on temperature. However, this does require additional a priori testing and parametrization effort.

B. Comparing Differently Aged Cells

In order to test if the battery parameter estimation algorithm adapts to aging behaviour, the three different datasets recorded at the three different aging stages of the cell are evaluated. The hypothesis is that when going from beginning-of-life towards end-of-life, the cell will display a decreasing capacity, represented by \hat{C}_0 and increasing resistance, represented by θ_2 and θ_3 . The resulting capacity estimates are displayed in Fig. 4 and show a clear distinction between the three different data sources. In all three cases, the first capacity update, after the first CC-charging session at $t = 4$ hr, establishes an estimate that is close to the final estimates, which are respectively 4.72 Ah (100%), 4.48 Ah (95.0%), and 4.33 Ah (91.7%). Furthermore, differences in the parameter estimates are observed between the different aging states in Fig. 5. Firstly, the SoC increase during charging is slightly larger on the aged cell, indicating a decreased capacity. Secondly, the average parameter values, are increasing with battery age. The average values are summarized in Table I. These confirm a plausible decreasing trend in the observed capacity and an increasing trend in the impedances.

C. Importance of Proper Segment-Selection

The proper selection of segments of data used to update the capacity estimate is imperative. All of the above results assume the complete charging segments as input to the RLS estimator, which is computationally practical and plausible assumption

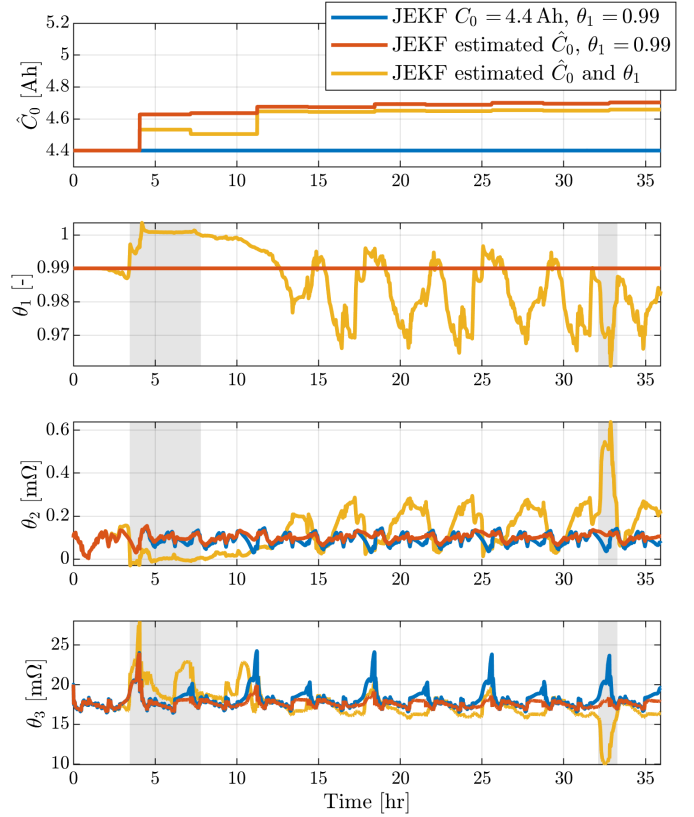


Fig. 3: The estimated capacity \hat{C}_0 and estimated JEFK parameters θ_1 , θ_2 , and θ_3 on 36 hours of WLTP data (beginning-of-life), both without and with capacity updates, and once with variable θ_1 . Regions where the JEFK is marginally stable are shaded.

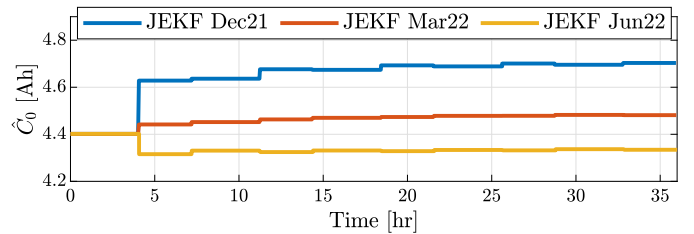


Fig. 4: The estimated capacity \hat{C}_0 based on 36 hours of WLTP data for three different aging states.

for an automotive use case. To emphasize the importance of this choice, the same framework, i.e., JEFK with RLS capacity estimation, is demonstrated in Fig. 6, yet with a different segment choice. In this case, a segment is ended as soon as

$$|\hat{s}_{b_i} - \hat{s}_{a_i}| > 0.2, \quad (9)$$

thereby also including discharging segments. The results indicate a capacity estimate which is more frequently updated, yet diverges from the expected value of 4.72 Ah.

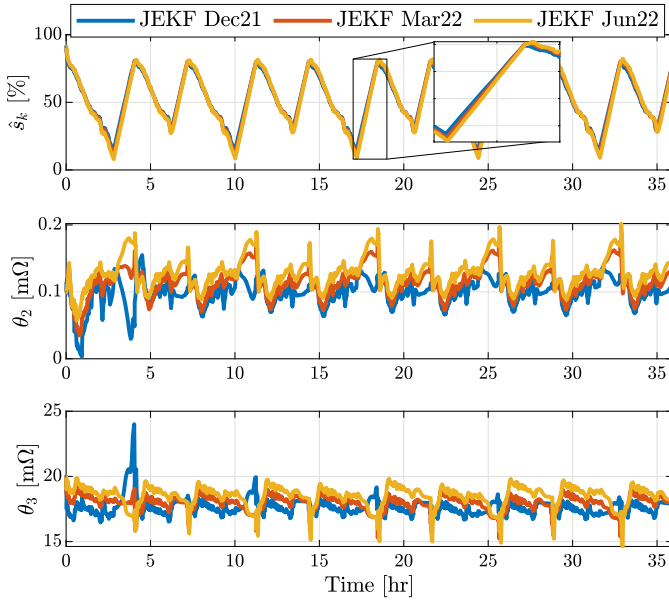


Fig. 5: The estimated SoC and JEFK parameters for three different aging states.

TABLE I: Estimated parameters based on data from different stadia of the cell's life, based on JEFK+RLS. Mentioned capacity is last value, impedance is averaged over 36 hr.

| Aging State | Capacity \hat{C}_0 [Ah] | θ_2 [m Ω] | θ_3 [m Ω] |
|---------------------|---------------------------|--------------------------|--------------------------|
| Beginning-of-life | 4.72 | 0.10 | 17.6 |
| Mid-life | 4.48 | 0.11 | 17.9 |
| Towards end-of-life | 4.33 | 0.13 | 18.5 |

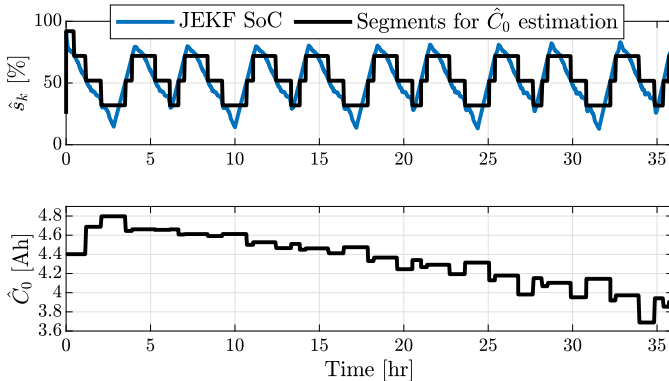


Fig. 6: Results of an alternative method where the segments used for capacity estimation are strictly segments of 20% SoC window. Data is from beginning-of-life.

IV. HARDWARE-IN-THE-LOOP IMPLEMENTATION

To demonstrate the application of the algorithm in real-world operating conditions, the JEFK+RLS algorithm is implemented as an algorithm in the Simulink-based TNO ADVANCE vehicle modeling environment [12]. The inputs to this control algorithm are current u_k and voltage y_k and the main outputs are JEFK-filtered voltage \hat{y}_k , SoC s_k , capacity \hat{C}_0 , θ_2 , and θ_3 . The TNO ADVANCE implementation allows the

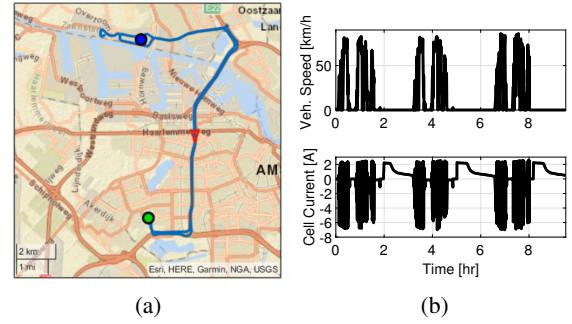


Fig. 7: The simulated route (a) and the resulting velocity profile and cell current (b).

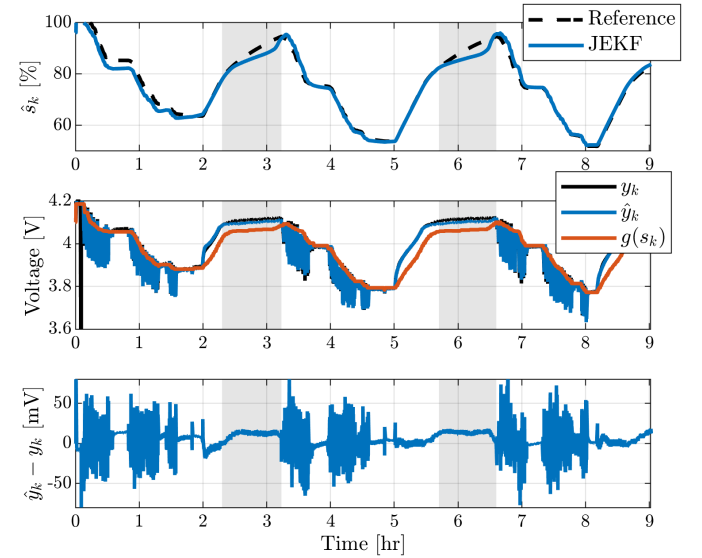


Fig. 8: The results of the HiL test with the estimated SoC s_k , a reference SoC obtained by coulomb-counting, the estimated open-circuit voltage $g(s_k)$, and the estimated terminal voltage \hat{y}_k with respect to the measured terminal voltage y_k . The shaded regions indicate the cv-stage of charging.

algorithm to be integrated into a vehicle powertrain simulation representing a battery-electric truck. A Hardware-in-the-Loop (HiL) test is performed, where a cell of the same type as described in Section III, at beginning-of-life-conditions, is subjected to drive cycles determined by the vehicle model, and the state estimates performed by the JEFK are used for vehicle control and charging-strategy decisions. A map of the vehicle route and the resulting current profile are shown in Fig. 7.

During the HiL test, the purpose of the algorithm is to provide an up-to-date SoC estimate for real-time control as well as to provide a continuously-adapted capacity \hat{C}_0 as input to charging strategies. Fig. 8 shows the estimated SoC and the corresponding measured and predicted terminal cell voltage. The figure shows that the SoC is generally accurate yet during charging deviations in SoC and terminal voltage can occur during the constant-voltage (cv) stage of charging. During these same periods, the parameter estimates θ_2 in Fig. 9

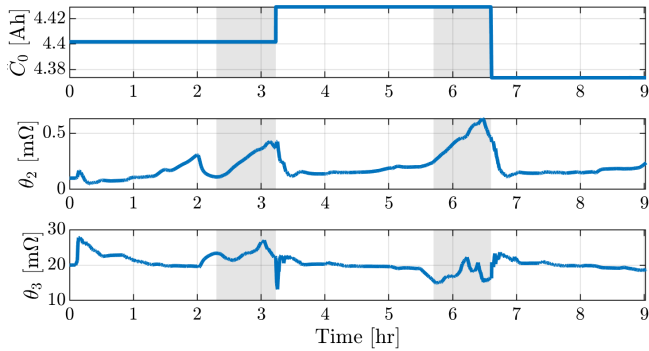


Fig. 9: The resulting capacity and impedance parameter estimates during the HiL test. The shaded regions indicate the cv-stage of charging.

are shown to deviate. The drifting of the JEKF is believed to be partly caused by the EMF being relatively flat around the 80 % SoC for this particular cell, in combination with the lack of dynamics in the current during charging. As a result, the JEKF estimates increasing impedance parameters instead of increasing the SoC to match the observed terminal voltage. This deviation is corrected as soon as discharging ends. Nevertheless, these deviations during charging will influence the estimated capacity and are considered a topic of future research.

V. CONCLUSIONS

This paper presents a combined method to estimate both battery capacity and impedance. The algorithm consists of a JEKF to estimate SoC and impedance, and an RLS algorithm that determines the capacity explicitly based on data from charging segments. By analyzing the algorithm on cell data with WLTP cycles it is shown that by adapting the capacity the RMS voltage error of the Kalman filter is reduced from 7.1 mV to 5.2 mV. The estimated capacity converges already after one CC charging session and the estimated capacity values follow a decreasing trend as the cell ages; from 4.72 Ah at beginning-of-life to 4.33 Ah near end-of-life. Accordingly, the instantaneous internal resistance of the cell is estimated to increase from 17.6 m Ω to 18.5 m Ω due to aging. Lastly, the algorithm is demonstrated in a HiL setup with a simulated vehicle and a physical cell.

Future work includes the implementation of the algorithm on embedded hardware and further research on the optimal se-

lection of the capacity-estimation segments. Additionally, extensions of the algorithm to include temperature-related effects should be considered, for instance by identifying temperature-dependent functions $f_i(\mathbf{p}_k)$ in the model description.

REFERENCES

- [1] X. Su, B. Sun, J. Wang, W. Zhang, S. Ma, X. He, and H. Ruan, "Fast capacity estimation for lithium-ion battery based on online identification of low-frequency electrochemical impedance spectroscopy and gaussian process regression," *Applied Energy*, vol. 322, p. 119516, 2022.
- [2] Z. Lyu, R. Gao, and X. Li, "A partial charging curve-based data-fusion-model method for capacity estimation of li-ion battery," *Journal of Power Sources*, vol. 483, p. 229131, 2021.
- [3] X. Sui, S. He, S. B. Vilsen, J. Meng, R. Teodorescu, and D.-I. Stroe, "A review of non-probabilistic machine learning-based state of health estimation techniques for Lithium-ion battery," *Appl. Energy*, vol. 300, p. 117346, Oct. 2021. [Online]. Available: <https://doi.org/10.1016/j.apenergy.2021.117346>
- [4] M. Wu, L. Wang, and J. Wu, "State of health estimation of the LiFePO4 power battery based on the forgetting factor recursive Total Least Squares and the temperature correction," *Energy*, vol. 282, p. 128437, Nov. 2023. [Online]. Available: <https://doi.org/10.1016/j.energy.2023.128437>
- [5] E. Bakas, B. Rosca, S. Wilkins, and T. Donkers, "Least-Squares-based Capacity Estimation for Lithium-ion Battery Cells," in *EEVC 2017*, Geneva, Switzerland, Mar. 2017, p. 6.
- [6] B. Jiang, H. Dai, X. Wei, and T. Xu, "Joint estimation of lithium-ion battery state of charge and capacity within an adaptive variable multi-timescale framework considering current measurement offset," *Appl. Energy*, vol. 253, p. 113619, Nov. 2019. [Online]. Available: <https://doi.org/10.1016/j.apenergy.2019.113619>
- [7] N. Janssen, "Extended State Estimation of a Lithium-Ion Battery Cell Using State-of-Health Estimation," Eindhoven, 2022, MSc. Thesis, Eindhoven Univ. of Tech. [Online]. Available: https://pure.tue.nl/ws/portalfiles/portal/218080877/1008382_ExtendedStateEstimation.pdf
- [8] H. Beelen, H. J. Bergveld, and M. C. F. Donkers, "Joint Estimation of Battery Parameters and State of Charge Using an Extended Kalman Filter: A Single-Parameter Tuning Approach," *IEEE Trans. Control Syst. Technol.*, vol. 29, no. 3, pp. 1087–1101, May 2021. [Online]. Available: <https://doi.org/10.1109/TCST.2020.2992523>
- [9] G. L. Plett, "Recursive approximate weighted total least squares estimation of battery cell total capacity," *J. Power Sources*, vol. 196, no. 4, pp. 2319–2331, Feb. 2011. [Online]. Available: <https://doi.org/10.1016/j.jpowsour.2010.09.048>
- [10] —, *Battery management systems, Volume II: Equivalent-circuit methods*. Artech House, 2015.
- [11] M. Paul-Henri and H. Vincent, "Robust and adaptive online state-of-health and state-of-charge estimation of li-ion battery cell," in *2023 IEEE Vehicle Power and Propulsion Conference (VPPC)*, Milan, Italy, Oct. 2023, p. 6.
- [12] E. van den Tillaart, S. Mourad, and H. Lupker, "TNO ADVANCE: a modular simulation tool for combined chassis and powertrain analysis," in *All Electric Combat Vehicle (AECV) Conference*, Noordwijkerhout, The Netherlands, Jan. 2002. [Online]. Available: <https://resolver.tno.nl/uuid:eee2b103-d626-4847-8af9-23eb7c5f0374>